RSC Advances

ROYAL SOCIETY OF CHEMISTRY

www.rsc.org/advances

Cite this: DOI: 10.1039/c0xx00000x

www.rsc.org/xxxxxx

ARTICLE TYPE

Mesoporous Carbon Coated Molybdenum Oxide Nanobelts for Improved Lithium Ion Storage

Ming Xu, Jing Tang, Hao Wu, and Gengfeng Zheng* [a]

Received (in XXX, XXX) Xth XXXXXXXXX 20XX, Accepted Xth XXXXXXXXX 20XX

DOI: 10.1039/b000000x

Nanocomposite composed of mesoporous carbon coated molybdenum oxide nanobelts are prepared and used as anode material for Li-ion batteries. The obtained MoO_x/meso-C nanocomposites provide a high surface area for electrochemical reaction, large mesopore channels for lithium ion transport, improved electrical conductivity, and structural flexibility for electrode volume change.

Mesoporous carbon is regarded as an excellent building block for developing hybrid nanomaterials, due to its ordered mesostructure, high surface area and excellent chemical stability,[1] and has been demonstrated as potential devices for adsorption,[2] catalysis,[3] energy conversion[4-5] and storage.[6] The open, interconnecting mesochannels with tunable pore size offer selective and fast ion transport; the high specific surface area provides abundant adsorption and reaction sites; and the continuous carbon framework allows for efficient charge transfer towards the supporting conductive substrates.[7] These structural characteristics are particularly attractive as lithium-ion battery (LIB) electrodes, while the theoretical capacity of graphite anode is relatively low (372 mAh/g).[8] On the other hand, many transition metal oxides, [9] such as molybdenum oxide (MoO_x), are promising lithium storage materials with a high theoretical capacity (e.g. 1117 mAh/g for MoO_3 and 838 mAh/g for MoO_2[10]) but MoO_3 shows low conductivity and poor stability.[11a] In the past several years, many reports have been demonstrated for improving the conductivity and lithium storage capacity of MoO_3 anodes, including the synthesis of nanoscale MoO_3 nanoparticles,[12] nanorods,[13] nanobelts[14] and nanowires,[15] direct growth of MoO_3 on conducting substrates,[11a] forming MoO_2/carbon nanowires by organic-inorganic assembly,[16] and *in-situ* reduction of MoO_2 with glucose[17a] and graphene.[17b]

As the main challenges for transition metal oxide-based LIB electrodes are the poor electrical conductivity and the capacity fading due to the electrode volume change during Li^+ insertion/extraction,[11] a mesoporous carbon layer coated on MoO_x nanostructures is expected to facilitate both the ion and charge transport towards the electrode surface, while at the same time providing structural flexibility to accommodate the large volume change of electroactive MoO_x anodes. Herein, we demonstrate the synthesis and electrochemical application of MoO_x nanobelts coated with mesoporous carbon. This synthesis is realized by the surface coating of a phenolic resol polymer on MoO_3 nanobelts *via* an evaporation induced self-assembly (EISA) process using amphiphilic block copolymer as a structural-directing agent, followed by thermal decomposition of polymer to form mesoporous carbon layers (Scheme 1). Compared to other methods of hybridizing with carbon such as graphene and carbon nanotubes, our approach is based on the solution-phase self-assembly of polymer precursors, which enables a conformal surface coating of MoO_3 nanobelts to efficiently reduce the aggregation, a problem often observed for metal oxides.[18] The obtained hybrid MoO_x/mesoporous carbon nanocomposite provides a high specific surface area for electrochemical reaction, large mesopore channel for lithium ion transport, improved electrical conductivity, and structural flexibility for volume change, leading to substantial enhancement of Li-ion storage capacity and cycling stability. Moreover, this EISA approach does not require designing specific synthetic routes for different host materials, and the use of resol as the mesoporous carbon precursors can fit for a large pH range of growth solutions. Therefore, this method can be served as a general means for surface functionalization/coating of a wide variety of transition metal oxides for the LIB use.

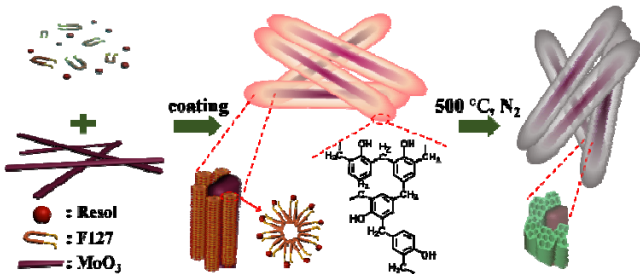

Scheme 1. Schematic illustration of the synthetic procedure for the MoO_x@meso-C composite.

MoO_3 nanobelts were synthesized by a hydrothermal process modified from a previous report.[19] In brief, $(NH_4)_6Mo_7O_{24}{\cdot}4H_2O$ and a block copolymer surfactant (Pluronic F127) were mixed in a HNO_3 solution, followed by incubation at 180 °C for 24 h (Experimental section, ESI). Scanning electron microscopy (SEM) images exhibit that the as-grown products have a long, belt-like morphology, with lengths of 5-20 μm (Fig. 1a). The cross-sections of these nanobelts have a rectangular shape, with width of 10-200 nm and thickness of 50-100 nm (Fig. 1b). No other shaped products were observed, indicating the high yield

and purity of our synthesis. Transmission electron microscopy (TEM) images of a typical MoO_3 nanobelt show a uniform width of ~ 100 nm, with flat surface and little amorphous surface layer (Fig. 1c). High-resolution TEM (HRTEM) image and the corresponding selected area electron diffraction (SAED) pattern reveals that this nanobelt is single crystalline with an orthorhombic α-MoO_3 phase (Fig. 1d).[20] The growth direction of this MoO_3 nanobelt is determined as [001]. Well-resolved lattice fringes corresponded to the *d*-spacing value of 0.38 nm, consistent with the (110) planes for single-crystal α-MoO_3 reported previously.[20] Energy dispersive X-ray spectroscopy (EDX) confirms the existence of Mo and O in the as-grown sample, with a Mo/O ratio of approximately 1:3 (Fig. S1).

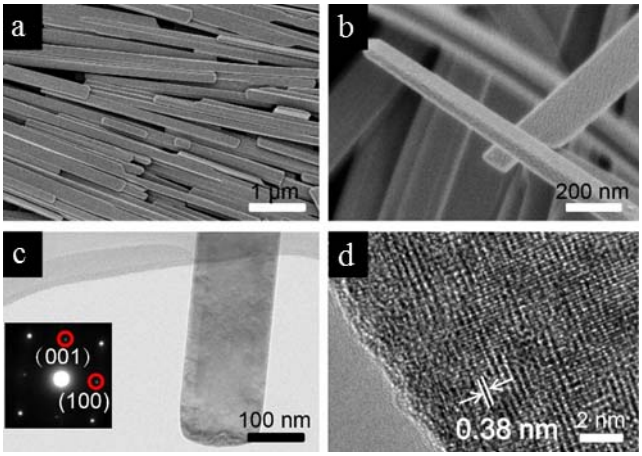

Fig. 1 a, b) SEM images of the as-grown MoO_3 nanobelts. c) TEM and d) HRTEM images of a typical MoO_3 nanobelt. Inset in (c): SAED pattern of this MoO_3 nanobelt.

Mesoporous carbon was coated on the MoO_3 nanobelts by a room-temperature EISA process,[7] in which the MoO_3 nanobelt powder was mixed with a resol precursor and Pluronic F127 triblock copolymer in an ethanol solution, followed by fast evaporation of ethanol and cross-linking of polymers (Experimental section). As the cross-linking of resol is not affected by the hydrolysis rate, this coating method can be applied to a large variety of precursor solutions and transition metal oxides. The samples were further calcined at 500 °C in N_2 to decompose the polymer into carbon, and a nanocomposite containing nanobelts and carbon coating was obtained (Fig. 2a, b and Fig. S2). The ratio between carbon and MoO_3 nanobelts is tuned by controlling tN2_he amount of resol precursor and surfactant added. The carbon matrix is composed of arrays of 1-dimensional (1D) oriented mesostructured channels between individual nanobelts. Some broken nanobelt structures can also be observed with the increase of the carbon coating amount, which are ascribed to the contraction of carbon structure during the calcination process. TEM images exhibit that at a low carbon coating amount, the nanobelts are covered by a thin amorphous layer (Fig. 2c). With the increase of the carbon coating amount, highly oriented 1D mesochannels with a pore size of ~ 11 nm are clearly observed between the nanobelts (Fig. 2d and Fig. S3), confirming the formation and coating of mesoporous carbon structures on the nanobelts. Here, in the condition of 0.3 g of MoO_3 with 2.0 g of phenolic resol (~ 5 % in ethanol), the average thickness of the coating carbon is about 100 to 200 nm.

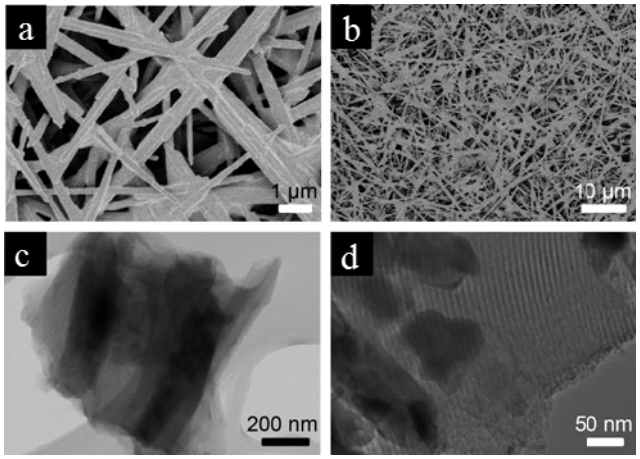

Fig. 2 a, b) SEM and c,d) TEM images of the MoO_x nanobelts coated with mesoporous carbon. The 1D mesopore channels of the mesoporous carbon are clearly observed.

X-ray diffraction (XRD) is used to characterize the crystal structure and phase purity of the obtained samples. The as-grown MoO_x nanobelts clearly display four well-resolved diffraction peaks in 2θ range of 20-70° (Fig. 3a). These peaks are associated with the 040, 060, 081 and 0100 reflections of anorthorhombic *α*-phase MoO_3 (JCPDS card No. 05-0508), which is also consistent with MoO_3 nanobelts reported previously.[21] No other diffraction peaks are detected, indicating the purity of the products. After being coated with mesoporous carbon, the original diffraction peaks disappear, and six new diffraction peaks associated with the -111, -211, -220, -312, 031 and -402 reflections of MoO_2 (JCPDS card No. 32-0671[22]) are observed, suggesting the reduction of Mo(VI) to Mo(IV) with mesoporous carbon located on the nanobelt surface. Thus, the composition of the hybrid nanocomposite is designated as MoO_x@meso-C, ($2 < x < 3$). In addition, the small-angle X-ray scattering (SAXS) patterns of the MoO_x@meso-C composites show two resolved scattering peaks, indexed as the 10 and 11 planes of a 2D hexagonal mesostructure (Fig. 3b), i.e., the space group *p6m*, consistent with FDU-15 mesoporous carbons.[1a]

The nitrogen sorption isotherms of the MoO_x@meso-C composites display typical type-*IV* curves with a H3 hysteresis loop (Fig. 3c), indicating the existence of mesoporous structure.[23] The specific surface area and the pore volume are calculated to be 147.4 m^2/g and 0.22 cm^3/g, respectively, which are substantially larger than those of as-grown MoO_3 nanobelts (4.8 m^2/g and 0.023 cm^3/g, respectively). The substantial increase of surface area and pore volume are mainly due to the contribution from the mesoporous carbon.[24] Moreover, a narrow pore size distribution is measured (inset in Fig. 3c), confirming the uniform mesopores of the carbon coating. The pore size calculated from the adsorption branch is ~ 12 nm, consistent with the TEM result.

The oxidation state change of molybdenum is further confirmed by the X-ray photoelectron spectroscopy (XPS). The pristine MoO_3 nanobelts display two distinctive peaks at ~ 232.5 and 235.6 eV (Fig. S4), attributed to Mo $3d_{3/2}$ and $3d_{5/2}$ of MoO_3, respectively.[25] After coated with mesoporous carbon, the XPS spectra can be fitted as four peaks at ~ 229.4, 233.1, 232.5 and

235.6 eV (Fig. 3d). The two peaks at 229.4 and 233.1 eV are attributed to the Mo 3d peaks of MoO_2, suggesting the conversion of Mo(VI) to Mo(IV) and in good accord with the results obtained from XRD patterns.[17] The other two peaks at 232.5 and 235.6 eV are affiliated to the Mo 3d peaks of MoO_3, which are ascribed to the re-oxidation of Mo(IV) to Mo(VI) in the air.[16a] In fact, the conductivity of MoO_2 is better than that of MoO_3.[16b] Thus, the valence state conversion of Mo will also contribute to the improved conductivity of the nanocomposites.

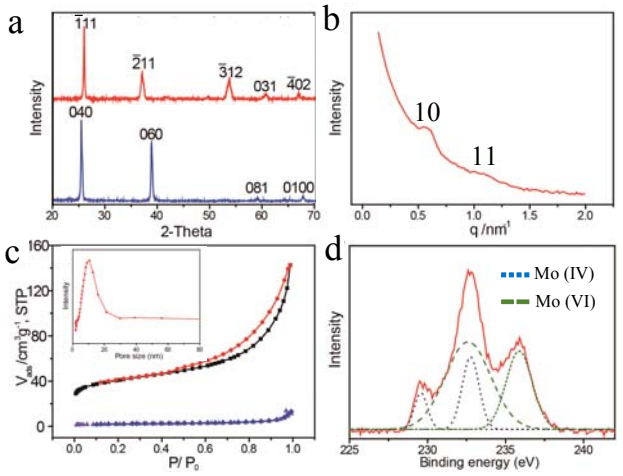

Fig. 3 a) XRD patterns of the MoO_3 nanobelts (lower) and MoO_x@meso-C nanocomposites (upper). b) SAXS pattern of the MoO_x@meso-C nanocomposites. c) N_2 sorption isotherms of the MoO_3 nanobelts (lower) and MoO_x@meso-C nanocomposite (upper). Inset is the pore size distribution of the MoO_x@meso-C nanocomposites. d) XPS spectra of MoO_x@meso-C nanocomposites, showing the Mo 3d peaks (red line). The decomposed lines represent Mo (IV) (blue dotted line) and Mo (VI) (green dashed line).

The electrochemical storage capacity of the synthesized hybrid MoO_x nanobelt coated with mesoporous carbon as LIB anodes is investigated based on the half-cell configuration. Pristine MoO_3 nanobelts and pure mesoporous carbon are also fabricated as anodes using a similar method for comparison. The electrochemical reaction is studied by the cyclic voltammetry (CV) measurement (Fig. 4a). A wide reduction peak near 0.5 V is observed during the first discharge cycle but absent in the following ones. This peak corresponds to the irreversible electrochemical reaction of forming a solid electrolyte interphase (SEI) layer on the electrode interface.[17] In addition, a small reduction peak at 1.1 V and an oxidation peak at 2.3 V are displayed, attributed to the reversible electrochemical reaction in the partially lithiated Li_xMoO_2 as Li^+ intercalation and deintercalation.[16]

Galvanostatic measurements of discharge/charge cycles are performed in a potential window of 3 − 0.01 V (vs. Li^+/Li) at a charge-discharge rate of 100 mA/g, and several representative cycles of the voltage-capacity characteristics, including the 1st, 2nd, 10th, and 30th ones, are selected to display (Fig. 4b). For the MoO_x@meso-C composite anode, one large plateau at ~ 0.5 V is observed during the first discharge cycle, which corresponds well with the CV measurement and is ascribed as the irreversible electrolyte reduction.[16-17] The initial discharge and charge capacities for the MoO_x@meso-C composite anode are 570 and 456 mAh/g, respectively, indicating ~ 20% irreversible capacity loss during the first cycle. For the pristine MoO_3 nanobelt anode (Fig. S5), a high initial discharge capacity of 1110 mAh/g is obtained, much higher than that of the MoO_x@meso-C composite, while the subsequent charging capacity significantly drops to 670 mAh/g, indicating ~ 40 % irreversible capacity lose during the first cycle.

The capacity retention of lithium storage is clearly demonstrated by summarizing the cycling performance of the MoO_x@meso-C anode (Fig. 4c). No significant capacity loss is observed since the second cycle, and the Coulombic efficiency is almost maintained as > 95 %. The discharge capacity is retained at 330 mAh/g after 40 cycles, corresponding to ca. 58% and 72% drop from the first and second discharge cycles, respectively. For comparison, the pristine MoO_3 nanobelt anode has a highest initial discharge capacity of 1110 mAh/g, while it quickly drops and retains at 208 mAh/g after 40 cycles, almost 89% loss from the initial value. The pure mesoporous carbon anode, on the other hand, has a relatively low initial discharge capacity of 666 mAh/g, which is almost kept constant at 190 mAh/g during the 2 − 40 cycles. As the mass and capacity of the MoO_x@meso-C anode includes contribution from both MoOx nanobelts and mesoporous carbon coating layer, it can be suggested that the mesoporous carbon coating on the MoO_x nanobelts surface, although lowering the initial anode capacity due to the lower lithium ion storage capability of carbon than MoO_x, can substantially improve the charge transport as well as the structural flexibility and stability, leading to better capacity retention of the hybrid nanocomposites during the Li^+ intercalation/deintercalation.

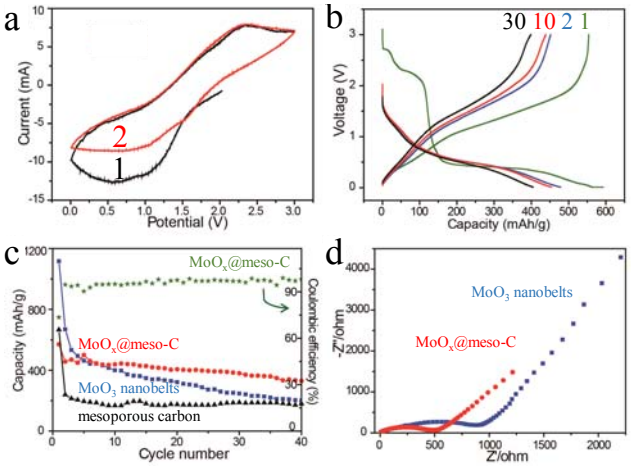

Fig. 4 a) Cyclic voltammetry plot of the MoO_x@meso-C nanocomposites for the 1st and 2nd cycles. b) Voltage profiles for the selected galvanostatic cycles of the MoO_x@meso-C nanocomposites for several selected cycles. c) Capacity versus cycle number for the MoO_x@meso-C nanocomposite (red), MoO_3 nanobelts (blue), and pure mesoporous carbon (black). d) Nyquist plots of the MoO_x@meso-C nanocomposite (red) and MoO_3 nanobelts (blue).

To illustrate the electrode capacity improvement, the electrochemical impedance spectroscopy (EIS) is carried out on

both the MoO_x@meso-C and pristine MoO_3 nanobelt samples. The Nyquist plot is acquired at a frequency range of 0.01 Hz − 100 kHz at an amplitude of 10 mV vs. the open circuit potential (Fig. 4d). Comparing to the pristine MoO_3 nanobelts, the MoO_x@meso-C anode displays an oblique straight line in the low frequency region with a similar slope but a shorter line, suggesting a faster Li^+ diffusion rate and smaller variation of the diffusion path enabled by the surface coating of mesoporous carbon.[26] This observation is expected, as the large mesopore size allows for efficient lithium ion transport, while the carbon framework serves as a structural spacer to prevent the aggregation of MoO_3 nanobelts. The semicircles in the high frequency region represent the charge transfer process in the electrode. The diameters of semicircles, which represents the total charge transport impedance of the electrodes,[17] are measured to be ~ 1000 and ~ 500 ohm for the pristine MoO_3 nanobelts and MoO_x@meso-C nanocomposites, respectively. The improvement of the conductivity is not only attributed to the carbonization of nanocomposite but also the transition of Mo(VI) to Mo(IV). Hence, the coating of mesoporous carbon on MoO_3 nanobelt surface improves the electrical conductivity, facilitates the charge transfer and reduces the contact resistance. Moreover, it also acts as a buffer that inhibits the volume expansion during the insertion/extraction of Li^+, thus enhancing the cycling performance.

In summary, we have demonstrated the self-assembly of the mesoporous carbon on MoO_3 nanobelt surface *via* EISA approach. The carbon coating on the nanobelts has a thickness of 100 − 200 nm with a pore size of 12 nm. Therefore, the obtained hybrid nanocomposites have a high specific surface area of 147.4 m^2/g for electrochemical reaction, large mesopore channel for Li^+ transport, improved electrical conductivity, and structural flexibility for volume change. LIB anodes made of the hybrid MoO_x nanobelt/mesoporous carbon composites show an enhanced lithium storage capacity as well as capacity retention. Our approach does not require any specific sample pre-treatment and can be applied in a large pH range of solutions, and thus may serve as a general method of interfacing a variety of transition metal oxide nanostructures with mesoporous carbon coating for efficient energy storage.

Acknowledgement

We thank the following funding agencies for supporting this work: the National Key Basic Research Program of China (2013CB934104), the Natural Science Foundation of China (21322311, 21071033), the Program for New Century Excellent Talents in University (NCET-10-0357), the Doctoral Fund of Ministry of Education of China, the Program for Professor of Special Appointment (Eastern Scholar) at Shanghai Institutions of Higher Learning, and the Deanship of Scientific Research of King Saud University (IHCRG#14-102).

Notes and references

[a] *Laboratory of Advanced Materials, Department of Chemistry, Fudan University, Shanghai, 200433, P. R. China. Fax/ Tel: (+86)21 5163 0352; E-mail: gfzheng@fudan.edu.cn*

† Electronic Supplementary Information (ESI) available: [details of the experimental section and supporting images]. See DOI: 10.1039/b000000x/

1 a) Y. Meng, D. Gu, F. Q. Zhang, Y. F. Shi, H. F. Yang, Z. Li, C. Z. Yu, B. Tu and D.Y. Zhao, *Angew. Chem. Int. Ed.*, 2005, **44**, 7053-7059; b) Q. F. Zhang, E. Uchaker, S. L. Candelariaza and G. Z. Cao, *Chem. Soc. Rev.*, 2013, **42**, 3127-3171.

2 a) X. Zhuang, Y. Wan, C. M. Feng, Y. Shen and D. Y. Zhao, *Chem. Mater.*, 2009, **21**, 706-716; b) G. J. Tao, L. X. Zhang, Z. L. Hua, Y. Chen, L. M. Guo, J. M. Zhang, Z. Shu, J. H. Gao, H. R. Chen, W. Wu, Z. W. Liu and J. L. Shi, *Carbon*, 2014, **66**, 547-559.

3 X. L. Ji, K. T. Lee, R. Holden, L. Zhang, J. J. Zhang, G. A. Botton, M. Couillard and L. F. Nazar, *Nat. Chem.*, 2010, **2**, 286-293.

4 Z. H. Wen and J. H. Li, *J. Mater. Chem.*, 2009, **19**, 8707-8713.

5 E. Ramasamy and J. Lee, *Chem. Commun.*, 2010, **46**, 2136-2138.

6 a) D. W. Wang, F. Li, M. Liu, G. Q. Lu and H. M. Cheng, *Angew. Chem., Int. Ed.*, 2008, **47**, 373-376; b) D. C. Guo, W. C. Li, W. Dong, G. P. Hao, Y. Y. Xu and A. H. Lu, *Carbon*, 2013, **62**, 322-329.

7 D. Feng, Y. Y. Lv, Z. X. Wu, Y. Q. Dou, L. Han, Z. K. Sun, Y. Y. Xia, G. F. Zheng and D. Y. Zhao, *J. Am. Chem. Soc.*, 2011, **133**, 15148-15156.

8 A. Mukhopadhyay, A. Tokranov, K. Sena, X. C. Xiao and B. W. Sheldon, *Carbon*, 2011, **49**, 2742-2749.

9 a) A. Q. Pan, H. B. Wu, L. Yu and X. W. (D) Lou, *Angew. Chem. Int. Ed.*, 2013, **125**, 2282-2286; b) J. X. Zhu, Z. Y. Yin, D. Yang, T. Sun, H. Yu, H. E. Hoster, H. H. Hng, H. Zhang and Q. Y. Yan, *Energy Environ. Sci.*, 2013, **6**, 987-993.

10 a) T. Tao, A. M. Glushenkov, C. F. Zhang, H. Z. Zhang, D. Zhou, Z. P. Guo, H. K. Liu, Q. Y. Chen, H. P. Hu and Y. Chen, *J. Mater. Chem.*, 2011, **21**, 9350-9355; b) Y. F. Shi, B. K. Guo, S. A. Corr, Q. H. Shi, Y. S. Hu, K. R. Heier, L. Q. Chen, R. Seshadri and G. D. Stucky, Nano *Lett.*, 2009, **9**, 4215-4220.

11 a) P. Meduri, E. Clark, J. H. Kim, E. Dayalan, G. U. Sumanasekera and M. K. Sunkara, *Nano Lett.*, 2012, **12**, 1784-1788; b) S. M. Xu, C. M. Hessel, H. Ren, R. B. Yu, Q. Jin, M. Yang, H. J. Zhao and D. Wang, *Energy Environ. Sci.*, 2014, **7**, 632-637; c) X. J. Hou, X. F. Wang, B. Liu, Q. F. Wang, Z. R. Wang, D. Chen and G. Z. Shen, *Chem Electro Chem*, 2014, **1**, 108-115; d) S. H. Lee, Y. H. Kim, R. Deshpande, P. A. Parilla, E. Whitney, D. T. Gillaspie, K. M. Jones, A. H. Mahan, S. Zhang and A. C. Dillon, *Adv. Mater.*, 2008, **20**, 3627-3632.

12 J. S. Chen, Y. L. Cheah, S. Madhavi and X. W. Lou, *J. Phys. Chem. C*, 2010, **114**, 8675-8678.

13 Y. S. Jung, S. Lee, D. Ahn, A. C. Dillon and S. H. Lee, *J. Power Sources*, 2009, **188**, 286-291.

14 a) Y. F. Dong, S. Li, H. M. Xu, M. Y. Yan, X. M. Xu, X. C. Tian, Q. Liu and L.Q. Mai, *Phys. Chem. Chem. Phys.*, 2013, **15**, 17165-17170; b) G. B. Wang , J. F. Ni, H. B. Wang and L. J. Gao, *J. Mater. Chem. A*, 2013, **1**, 4112-4118; c) M. F. Hassan, Z. P. Guo, Z. Chen, H. K. Liu, *J. Power Sources*, 2010, **195**, 2372-2376.

15 a) Z. Q. Yuan , L. L. Si , D. H. Wei , L. Hu , Y. C. Zhu , X. N. Li and Y. T. Qian, *J. Phys. Chem. C*, 2014, DOI: 10.1021/jp410550v; b) L. Zhou, L. C. Yang, P. Yuan, J. Zou, Y. P. Wu and C. Z. Yu, *J. Phys. Chem. C*, 2010, **114**, 21868-21872.

16 a) Q. S. Gao, L. C. Yang, X. C. Lu, J. J. Mao, Y. H. Zhang, Y. P. Wu and Y. Tang, *J. Mater. Chem.*, 2010, **20**, 2807-2812; b) B. Hu, L. Q. Mai, W. Chen and F. Yang, *ACS Nano*, 2009, **3**, 478-482.

17 a) L. C. Yang, L. L. Liu, Y. S. Zhu, X. J. Wang and Y. P. Wu, *J. Mater. Chem.*, 2012, **22**, 13148–13152; b) Y. M. Sun, X. L. Hu, W. Luo and Y. H. Huang, *ACS Nano*, 2011, **5**, 7100-7107.

18 H. B. Wu, J. S. Chen, H. H. Yang and X. W. Lou, *Nanoscale*, 2012, **4**, 2526-2542.

19 R. L. Liang, H. Q. Cao and D. Qian, *Chem. Commun.*, 2011, **47**, 10305-10307.

20 L. Q. Mai, B. Hu, W. Chen, Y. Y. Qi, C. S. Lao, R. S. Yang, Y. Dai and Z. L. Wang, *Adv. Mater.*, 2007, **19**, 3712-3716.

21 G. C. Li, L. Jiang, S. P. Pang, H. R. Peng and Z. K. Zhang, *J. Phys. Chem. B*, 2006, **110**, 24472-24475.

22 B. Hu, L. Q. Mai, W. Chen and F. Yang, *ACS Nano*, 2009, **3**, 478-482.
23 X. Du and J. H. He, *Langmuir*, 2011, **27**, 2972-2979.
24 Y. P. Zhai, Y. Q. Dou, X. X. Liu, B. Tu and D. Y. Zhao, *J. Mater. Chem.*, 2009, **19**, 3292-3300.
25 B. Yan, Z. Zheng, J. X. Zhang, H. Gong, Z. X. Shen, W. Huang and T. Yu, *J. Phys. Chem. C*, 2009, **113**, 20259-20263.
26 B. Liu, H. T. Yuan and Y. S. Zhang, *Int. J. Hydrogen. Energ.*, 2004, **29**, 453-458.